

1 **Identifying uncertainties in hydrologic fluxes and seasonality from**  
2 **hydrologic model components for climate change impact**  
3 **assessments**

4 Dongmei Feng<sup>1\*</sup> and Edward Beighley<sup>2,3</sup>

5 <sup>1</sup> Civil and Environmental Engineering, University of Massachusetts, Amherst, MA, USA

6 <sup>2</sup> Civil and Environmental Engineering, Northeastern University, MA, USA

7 <sup>3</sup> Marine and Environmental Sciences, Northeastern University, MA, USA

8 \*Corresponding author, email address: [dmei.feng@gmail.com](mailto:dmei.feng@gmail.com), telephone: (617) 697-8789

9 **Abstract:** Assessing impacts of climate change on hydrologic systems is critical for developing  
10 adaptation and mitigation strategies for water resource management, risk control and ecosystem  
11 conservation practices. Such assessments are commonly accomplished using outputs from a  
12 hydrologic model forced with future precipitation and temperature projections. The algorithms  
13 used for the hydrologic model components (e.g., runoff generation) can introduce significant  
14 uncertainties in the simulated hydrologic variables. Here, a modeling framework was developed  
15 that integrates multiple runoff generation algorithms with a routing model and associated  
16 parameter optimizations. This framework is able to identify uncertainties from both hydrologic  
17 model components and climate forcings as well as associated parameterization. Three  
18 fundamentally different runoff generation approaches: runoff coefficient method (RCM,  
19 conceptual), variable infiltration capacity (VIC, physically-based, infiltration excess) and simple-  
20 TOPMODEL (STP, physically-based, saturation excess), were coupled with the Hillslope River  
21 Routing model to simulate surface/subsurface runoff and streamflow. A case study conducted in  
22 Santa Barbara County, California, reveals increased surface runoff in February and March while  
23 decreased runoff in other months, a delayed (3 days, median) and shortened (6 days, median) wet  
24 season, and increased daily discharge especially for the extremes (e.g., 100-yr flood discharge,  
25  $Q_{100}$ ). The Bayesian Model Averaging analysis indicates the probability of such increase can be  
26 up to 85%. For projected changes in runoff and discharge, general circulation models (GCMs)  
27 and emission scenarios are two major uncertainty sources, accounting for about half of the total  
28 uncertainty. For the changes in seasonality, GCMs and hydrologic models are two major  
29 uncertainty contributors (~35%). In contrast, the contribution of hydrologic model parameters to  
30 the total uncertainty of changes in these hydrologic variables is relatively small (<6%), limiting  
31 the impacts of hydrologic model parameter equifinality in climate change impact analysis. This  
32 study provides useful information for practices associated with water resources, risk control and  
33 ecosystems conservation and for studies related to hydrologic model evaluation and climate  
34 change impact analysis for the study region as well as other Mediterranean regions.

## 35 **1. Introduction**

36 Streamflow is essential to human and ecosystems, supporting human's life and economic  
37 activities, providing habitat for aquatic creatures, and exporting sediment/nutrients to coastal  
38 ecosystems (Feng et al., 2016; Barnett et al., 2005; Milly et al., 2005). Understanding streamflow  
39 characteristics is important for water-resources management, civil infrastructure design and  
40 making adaptation strategies for economic and ecological practices (Feng et al., 2019). With  
41 economic development and population growth, the emission of greenhouse gas is likely to  
42 increase during 21<sup>st</sup> century (IPCC, 2014). The increase in global surface temperature is  
43 projected to exceed 2°C by the end of 21<sup>st</sup> century even under moderate emission scenarios (e.g.,  
44 Representative Concentration Pathways, RCPs, 4.5 and 6.0) (IPCC, 2014). Intensified hydro-  
45 meteorological processes, altered precipitation forms and patterns, and intensified atmospheric  
46 river events and oceanic anomalies (e.g. El Nino events) are projected and likely to cause  
47 substantial impacts on hydrologic fluxes (Barnett et al., 2005; Tao et al., 2011; Dai,  
48 2013; Dettinger, 2011; Vicky et al., 2018; Cai et al., 2014; Feng et al., 2019).

49 The integration of climate projections and hydrologic models enables the investigation of  
50 hydrologic dynamics under the future climate conditions. However, the simulated hydrologic  
51 fluxes contain uncertainties from various sources. Due to the epistemic limitations (e.g., human's  
52 lack of knowledge about hydrologic processes and boundary conditions) and the complexities in  
53 nature (e.g., temporal and spatial heterogeneity), hydrologic models are simplified  
54 representations of natural hydrologic processes (Beven and Cloke, 2012). Generally, hydrologic  
55 models have modules simulating water partitioning at land surface (named as runoff generation  
56 process in this study), evapotranspiration (ET), and water transportation along terrestrial  
57 hillslopes and channels (named as routing process here). Each process can be represented in  
58 different ways, which thus results in uncertainties in simulated variables. For the runoff  
59 generation process, surface runoff is mainly represented as infiltration excess overland flow (or  
60 Hortonian flow (Horton, 1933)) or saturation excess overland flow. Infiltration excess overland  
61 flow occurs when water falls on the soil surface at a rate higher than that the soil can absorb.  
62 Saturation excess overland flow occurs when precipitation falls on completely saturated soils.  
63 Surface runoff can also be quantified conceptually, for example, a runoff coefficient can be used  
64 to generate surface runoff as a proportion of precipitation rate. Subsurface runoff is generally

65 represented as functions of soil characteristics and topographic features. The complexity of these  
66 functions varies significantly, from simple linear to combinations of multiple non-linear.  
67 Parameterization can be another uncertainty source. Due to the nonlinearity of hydrologic  
68 processes, different combinations of model parameters can achieve similar, if not identical,  
69 model performance. Model parameter selections based on calibration metrics can result in  
70 different optimal parameter values (i.e., parameter equifinality). When it comes to hydrologic  
71 impact assessments, the climate forcings, which differ among General Circulation Models  
72 (GCMs) due to the model discrepancy and the uncertainty of future emission scenarios, also  
73 contribute to the uncertainties in hydrologic simulations. Without appropriate assessment of  
74 these uncertainties, standalone studies on the climate change impacts can be difficult to interpret.  
75 Systematic assessments of the relevant uncertainties associated with simulated hydrologic fluxes  
76 are needed.

77       Some studies have been performed to investigate uncertainties mentioned above at both  
78 variable scales (for example, (Wilby and Harris, 2006;Vetter et al., 2015;Valentina et al.,  
79 2017;Kay et al., 2009;Eisner et al., 2017;Su et al., 2017;Schewe et al., 2014;Hagemann et al.,  
80 2013;Asadih and Krakauer, 2017;Chegwidden et al., 2019;Hattermann et al., 2018;Addor et al.,  
81 2014;Vidal et al., 2016;Giuntoli et al., 2018;Alder and Hostetler, 2019)). Most previous studies  
82 treated hydrologic models as a whole package. However, hydrologic models consist of multiple  
83 components (e.g., runoff generation, ET and routing). These components can be significantly  
84 different among models. When considering the hydrologic model as a whole, it is difficult to  
85 quantify relative uncertainty contributions from different components. Troin et al. (2018) tested  
86 the uncertainties from hydrologic model components for snow and potential ET. In this study, a  
87 consistent hydrologic modeling framework that integrates multiple runoff generation process  
88 models with surface, subsurface and channel routing processes and associated parameter  
89 uncertainties was developed. This framework enables uncertainties from different components  
90 representing hydrologic processes and associated model parameters as well as model forcings  
91 (e.g., precipitation and temperature) to be quantified and compared in a consistent manner. In  
92 this framework, three runoff generation process models which represent three fundamentally  
93 different approaches mentioned above were used. The conceptual frameworks were adapted from  
94 the variable infiltration capacity model (Wood et al., 1992;Liang et al., 1996) (infiltration  
95 excess), simple-TOPMODEL (Niu et al., 2005;Beven et al., 1995;Beven, 2000) (saturation

96 **excess**), and the runoff coefficient method (Feng et al., 2019) (conceptual). Each approach was  
97 coupled within one routing model (i.e., Hillslope River Routing model, HRR (Beighley et al.,  
98 2009)) to simulate the terrestrial hydrological processes. This modeling framework was also  
99 integrated with a Bayesian model averaging (BMA) analysis to assess the performance of  
100 different model-forcing-parameter combinations and to provide actionable information (e.g.,  
101 probability of estimated changes) for associated practices, such as water resource management  
102 and ecology conservation.

103 A case study was presented for Santa Barbara County (SBC), CA, a biodiverse region  
104 under a Mediterranean climate with a mix of highly developed and natural watersheds. Previous  
105 studies (e.g., Feng et al., 2019) showed that the intensified storm events concentrated in a shorter  
106 and delayed wet season in SBC under future climate conditions will cause significant increase in  
107 discharge, especially the extremes (e.g., 100-yr discharge). The climate change impacts on the  
108 path and quantity of surface/subsurface runoff and discharge will impact the soil erosion,  
109 sediment/nutrients transport and subsequently affect the coastal ecosystems (Myers et al., 2019)  
110 Feng et al., 2019). The longer dry season may also contribute to the increased occurrence of  
111 droughts and wildfires (Myers et al., 2019). Therefore, changes in these hydrologic variables  
112 (e.g., runoff, discharge and seasonality) under future climate conditions and associated  
113 uncertainties are essential to assess the vulnerability of coastal region in CA and make adaptation  
114 strategies to accommodate climate change. In this study, we simulated future hydrologic  
115 variables using three hydrologic models forced with climate outputs from 10 GCMs that were  
116 selected for their good performance in representing historical meteorological characteristics in  
117 the study region, under 2 emission scenarios (RCP 4.5 and RCP 8.5) (Feng et al., 2019). The  
118 main objectives of this study were to: (1) evaluate and compare the performance of hydrologic  
119 models with different approaches representing runoff generation process using a consistent  
120 modeling framework; (2) quantify the relative contributions of different sources (including  
121 hydrologic process models, parameterizations, GCM forcings and emission scenarios) to the total  
122 uncertainty in simulated surface/subsurface runoff, streamflow, and seasonality; and (3) provide  
123 actionable information and suggestions for studies and practices associated with hydrologic  
124 impacts of climate change.

## 125 **2. Methods**

### 126 **2.1 Study region**

127 The study region is located in coastal Santa Barbara County (SBC), California, where  
128 watersheds drain into the Santa Barbara Channel from just west of the Ventura River to just east  
129 of Point Conception (Figure 1). The combined land area is roughly 750 km<sup>2</sup> with 135 watersheds  
130 ranging from 0.1 to 123 km<sup>2</sup>. The local climate is Mediterranean, with an average annual  
131 precipitation of roughly 600 mm (Feng et al., 2019). Most of the annual precipitation occurs in  
132 fall/winter with 85% of rainfall occurring in the November-March period. Thus, it is  
133 characterized by the intense and flashy floods in winter time. More than 80% of annual discharge  
134 occurs in only a few number of large events during January-March and a large fraction of annual  
135 discharge happens within one day (Beighley et al., 2003). River channels are typically filled with  
136 sediment during dry season (April-October) and are scoured with the initiation of wet season  
137 floods (Scott and Williams, 1978; Keller and Capelli, 1992). River flow is the major source of  
138 sediment exported to the coastal sandy beaches in SBC. Therefore, the timing of seasonality,  
139 path of runoff, and magnitudes of flood events are critical to both local community and coastal  
140 ecosystems.

### 141 **2.2 Data**

142 Daily precipitation and temperature with a spatial resolution of 0.0625° x 0.0625°  
143 (roughly 6 by 6 km) (Livneh et al., 2015), and daily streamflow from 4 USGS gauges for the  
144 period 1984-2013 were used to calibrate and validate the hydrologic models. The Global Soil  
145 Dataset for use in Earth system models (GSDE) was used to estimate saturated hydraulic  
146 conductivity and saturated moisture content. The 16-day composite albedo product (MCD43C3)  
147 with a spatial resolution of 0.05° x 0.05° and the monthly aerosol optical depth product  
148 (MOD08M3) with a spatial resolution of 1.0° x 1.0° both derived from NASA's Moderate  
149 Resolution Imaging Spectroradiometer (MODIS) were used to determine net radiation for  
150 evapotranspiration (PET) estimation. The aerosol optical depth product was downscaled to 0.05°  
151 x 0.05° (Raoufi and Beighley, 2017).

152 For the historical (1986-2005) and future climate simulations (2081-2100), downscaled  
153 precipitation and temperature from ten climate models (please refer to Pierce et al. (2014) and  
154 Pierce et al. (2015) for model details) in Coupled Model Inter-Comparison Project, Phase 5,  
155 (CMIP5) (Taylor et al. 2012) for two emission scenarios RCP 4.5 and RCP 8.5 (Moss et al.  
156 2010) were used. These 10 GCMs were selected because they have the best performance in  
157 representing historical climate dynamics at southwest U.S. and California state scales (Pierce et  
158 al., 2018).

## 159 2.3 Hydrologic modeling framework

### 160 2.3.1 Hydrologic model development

161 This modeling framework was developed on the basis of the Hillslope River Routing  
162 model (HRR) (Beighley et al., 2009). The watersheds were delineated using **the Digital Elevation**  
163 **Model (DEM) data with a resolution of 3" (~90 m at the equator) (Yamazaki et al., 2017)**. The  
164 sub-basins were irregular-shape catchments defined by the flow accumulation area threshold. In  
165 this study, the threshold was 1 km<sup>2</sup>, which means the sub-basins (model units) were in size of  
166 roughly 1 km<sup>2</sup>. The hydrogeological inputs of hydrologic models, including surface roughness,  
167 saturated hydraulic conductivity, soil thickness, porosity, plane slope, channel slope and channel  
168 roughness, were averaged over each sub-basin. This indicates these parameters were averaged  
169 for each model unit, the majority of which has an area of roughly 1 km<sup>2</sup>, with less than 1%  
170 having an area of <1 km<sup>2</sup>. The geometry of each sub-basin (plane length and width) was  
171 calculated based on an “open-book” assumption, which assumes each sub-basin is a rectangular  
172 divided by the river channel into two identical parts like an open book. Please refer to Beighley  
173 et al. (2009) for more details. The grid-based potential ET (PET) was estimated using the method  
174 of Raoufi and Beighley (2017). The precipitation and PET were extracted for each sub-basin  
175 using an area-weighted average method. Then the water-balance model (i.e., runoff generation  
176 method) was applied to each model unit to simulate runoff generation processes. Here, three  
177 runoff generation methods: runoff coefficient (Feng et al., 2019), and the methods used in  
178 Variable Infiltration Capacity (VIC) (Wood et al., 1992;Liang et al., 1996) **and simple-**  
179 **TOPMODEL model (Niu et al., 2005;Beven, 2000;Beven et al., 1995)**, were used to simulate the  
180 generation of surface and subsurface runoff excess. The routing methods within the HRR model  
181 (i.e., kinematic wave for surface and subsurface lateral routing and Muskingum-Cunge for

182 channel routing) were used to simulate the transport of runoff excess. To clarify, we denote the  
183 three runoff generation algorithms: runoff coefficient, runoff generation method used in Variable  
184 Infiltration Capacity and runoff generation method used in simple-TOPMODEL as RCM, VIC  
185 and STP, respectively. Three hydrologic models which integrate one of these runoff generation  
186 methods with HRR routing model are referenced as RCM-HRR, VIC-HRR and STP-HRR,  
187 respectively. The differences between simulations from these three models were considered as  
188 the uncertainty resulting from hydrologic models. The three runoff generation algorithms were  
189 described in the Supplemental material.

190 The water movement between soil layers in the soil matrix was similar to that in the  
191 modified VIC-2L model (Liang et al., 1996). The soil was divided into 2 layers: upper layer (0.6  
192 m) and lower layer (1.2 m). The soil thickness data was from the Soil Survey Geographic  
193 (SSURGO) Data Base for Santa Barbara County (NRCS, 1995). After the surface runoff was  
194 determined, the infiltrated water was added to the upper soil layer, and the soil moisture was  
195 updated. If the upper soil was oversaturated, the excess water was returned to surface. The  
196 evapotranspiration was estimated using Eq. S15. The interaction between upper and lower soil  
197 layers was simulated using the Clapper-Hornberger equation (Eq. S16-S17). Subsurface runoff  
198 was generated from the bottom of the lower soil layer. After the water fluxes (runoff, ET and  
199 water movement between soil layers) were determined, the soil moisture was updated which  
200 would be used for the water balance calculation in the next time step. After water excess for  
201 surface and subsurface runoff was quantified, the kinematic wave approach was applied to  
202 simulate the transport of runoff from the planes (surface and subsurface), and the Muskingum  
203 Cunge method was used for channel routing following the conservation equations (Eq.S18-S20)  
204 (Beighley et al., 2009). Two conceptual parameters  $K_{s\_all}$  and  $K_{ss\_all}$  were used in the routing  
205 model, to account for spatial heterogeneity at the model unit scale and uncertainties in the hydro-  
206 geologic inputs associated with the plane routing processes (e.g., surface roughness and saturated  
207 hydraulic conductivity). A conceptual illustration of the hydrologic models is shown in Figure 2.

### 208 2.3.2 Model calibration

209 After the models were setup, a state-of-the-art optimization algorithm, Borg  
210 Multiobjective Evolutionary Algorithm (Borg MOEA) (Hadka and Reed, 2013), was adopted to

211 optimize the model parameters (Table 1). The models spun up for one year to ensure the  
 212 equilibrium status. For each model, there were 4 parameters calibrated for runoff generation  
 213 processes and 2 parameters calibrated for routing processes.  $K_{s\_all}$  and  $K_{ss\_all}$  are conceptual  
 214 parameters, and they can be different for different model structures even for the same study  
 215 region. Therefore, they were calibrated for each model separately. The Nash–Sutcliffe model  
 216 efficiency coefficient (NSE) (Eq. (1)) was used to assess model performance, as it accounts for  
 217 model performance in terms of both timing and magnitudes of peak flow and base flow that are  
 218 particularly important in this study. The optimal parameter set was determined after the  
 219 improvement of error was minimized (here it was defined as  $\Delta NSE < 0.005$ ).

$$NSE = 1 - \frac{\sum_{t=1}^T (Q_s^t - Q_o^t)^2}{\sum_{t=1}^T (Q_o^t - \overline{Q_o})^2} \quad (1)$$

220 where  $Q_s^t$  and  $Q_o^t$  are simulated and observed discharge at time t, respectively, ( $m^3 s^{-1}$ );  
 221 and  $\overline{Q_o}$  is the mean observed discharge during the study period of length T, ( $m^3 s^{-1}$ ).

222 To quantify the uncertainties from model parameters, we selected 10 parameter sets using  
 223 the following criteria: (1) select 4 parameter sets with highest NSE based on the calibration  
 224 results; (2) rank the rest parameter sets based on their performance (i.e., NSE), and randomly  
 225 select 6 sets from the top 20% candidates. This parameter selection process enabled us to take  
 226 both parameter dominance and variability into account, while maintaining the high model  
 227 performance, which is important for the uncertainty analysis. These 10 parameter sets were then  
 228 used for uncertainty analysis.

## 229 2.4 Uncertainty Analysis

230 The uncertainty was quantified by running each of the 30 hydrologic model-parameter  
 231 sets (i.e., 3 hydrologic models and 10 parameter sets,  $3 \times 10 = 30$ ) with each of the 20 forcing sets  
 232 (i.e., 10 GCMs and 2 emission scenarios,  $10 \times 2 = 20$ ) for a total of 600 simulations. Here, we used  
 233 GCM outputs as the forcings of hydrologic models for both historical (1986-2005) and future  
 234 (2081-2100) periods. For each simulation scenario (i.e., the combination of hydrologic model,  
 235 parameter set, GCM and RCP), the historical and future daily streamflow and runoff were  
 236 simulated, and the relative changes (%) were quantified. Note, there is no RCPs for historical  
 237 period, and we used the same historical simulation for RCP 4.5 and 8.5. To evaluate the



238 uncertainty sources and their relative significance in these simulated changes in runoff, discharge  
 239 and seasonality for the future period, the analysis of variance (ANOVA) (Vetter et al.,  
 240 2015;Addor et al., 2014;Hattermann et al., 2018;Chegwidden et al., 2019) was used. The  
 241 contribution of each uncertainty source for a variable of interest (e.g., monthly runoff, 100-yr  
 242 flood discharge or the duration of wet season) was defined as the fraction of its variance to the  
 243 total variance. The total variance was quantified as the total sum of squares ( $SS_{Total}$ ) of  
 244 differences between the simulations and the mean of all simulations (Eq. (2)):

$$SS_{Total} = \sum_{i=1}^{N_{Hyd}} \sum_{j=1}^{N_{para}} \sum_{k=1}^{N_{GCM}} \sum_{l=1}^{N_{RCP}} (q_{ijkl} - q_{0000})^2 \quad (2)$$

245 where  $q_{ijkl}$  is the simulated value of the variable of interest by  $i^{th}$  hydrologic model with  $j^{th}$   
 246 parameter set, forced by  $k^{th}$  GCM projection under  $l^{th}$  RCP scenario;  $q_{0000}$  is the overall average  
 247 of the simulated variable. Next, the  $SS_{Total}$  can be divided into 15 parts representing the 4 main  
 248 effects (or first-order effects), 6 second-order, 4 third-order and 1 fourth-order interaction effects.  
 249 For clarity, the third and fourth orders of interaction effects were combined and represented as  
 250  $SS_{3,4}$  in Eq. (3).

$$\begin{aligned} SS_{Total} = & SS_{Hyd} + SS_{para} + SS_{GCM} + SS_{RCP} + SS_{Hyd.para} + SS_{Hyd.GCM} \\ & + SS_{Hyd.RCP} + SS_{para.GCM} + SS_{para.RCP} + SS_{GCM.RCP} \\ & + SS_{3,4} \end{aligned} \quad (3)$$

251 where  $SS_{Hyd}$ ,  $SS_{para}$ ,  $SS_{GCM}$  and  $SS_{RCP}$  are the main effects (i.e., uncertainties or variance) from  
 252 hydrologic models, hydrologic model parameters, GCMs and RCPs, respectively;  
 253  $SS_{Hyd.para}$ ,  $SS_{Hyd.GCM}$ ,  $SS_{Hyd.RCP}$ ,  $SS_{para.GCM}$ ,  $SS_{para.RCP}$  and  $SS_{GCM.RCP}$  are uncertainties  
 254 from interactions between the hydrologic models and parameterization, hydrologic models and  
 255 GCMs, hydrologic models and RCPs, parameterization and GCMs, parametrization and RCPs,  
 256 and GCMs and RCPs, respectively. The calculation of each order is illustrated in Eq. S21-S23.

257 To avoid bias from the difference in sample sizes of uncertainty sources (i.e., 3  
 258 hydrologic models, 3 parameter sets, 10 GCMs and 2 RCPs), a subsampling step was performed  
 259 by following Vetter et al. (2015). In the subsampling step, 2 samples (i.e., the minimum number

260 of uncertainty source, here it is RCPs) from each source were randomly selected, that is, 2  
261 hydrologic models, 2 parameter sets, 2 GCMs and 2 RCPs, which indicates  $N_{Hyd}$ ,  $N_{para}$ ,  $N_{GCM}$   
262 and  $N_{RCP}$  in Eq. (2), (S21)-(S23) are all equal to 2. This generated  $C_3^2 \times C_{10}^2 \times C_{10}^2 \times C_2^2=6075$   
263 subsamples. For each subsample, the fractional sum of squares was calculated for each effect  
264 using Eq. S21-S23, and then the average of variance fractions of each source is used as the  
265 uncertainty contribution from that source using Eq. S24.

## 266 2.5 Probability of estimated changes

267 In addition to quantifying uncertainties and associated contributions from different  
268 sources, an evaluation on the probability of uncertain changes in discharge can be useful to  
269 provide actionable information for the stakeholders such as water resource managers. In this  
270 study, the Bayesian model averaging (BMA) (Duan et al., 2007) was used to evaluate the model  
271 performance in reproducing historical hydrologic conditions, and then weights were assigned to  
272 each of them based on their performance. A model with better performance was assigned a  
273 higher weight, assuming it has a higher probability to represent the truth. Note, there is no RCPs  
274 for historical period, so only combinations of hydrologic models, parameter sets and GCMs  
275 ( $3 \times 10 \times 10=300$ ) were evaluated. Here the models' performance in representing annual mean  
276 discharge ( $Q_m$ ) and annual maximum daily discharge ( $Q_p$ ) is evaluated. Here, the annual mean  
277 discharge was defined as the average of daily streamflow in a year. **In this study region, there is**  
278 **typically no rain for most time of a year, and it is not uncommon in such a Mediterranean climate**  
279 **region that the annual runoff is mainly generated from one major storm event. Therefore, the**  
280 **annual mean/max series are representative of the characteristics of the discharge dynamics.** The  
281 details of this procedure can be found in the Supplemental material. After the weights of model  
282 ensemble were obtained using the BMA method, the statistics of posterior probability  
283 distribution (here it was assumed to be normal distribution) of estimated changes in  $Q_m$ ,  $Q_p$  and  
284  $Q_{100}$  in the future (2081-2100) relative to historical period 1986-2005 were calculated using Eq.  
285 S29-S34.

## 286 2.6 Definition of hydrologic seasonality

287 To quantify the onset and duration of hydrologic seasons, we calculated the accumulative  
288 discharge in the whole basin for each water year. Then the day showing the 10% of accumulative

289 annual discharge was defined as the onset of the wet season, and the number of days between the  
290 10 and 90% of the accumulated discharge series was defined as the duration of the wet season.

## 291 **3. Results and Discussion**

### 292 **3.1 Hydrologic model performance**

293 The three hydrologic models performed well in representing streamflow dynamics in the study  
294 region. The NSE varies within 0.56-0.67 and 0.53-0.62 for calibration and validation periods,  
295 respectively, in Mission Creek (USGS gauge NO. 11119750) (Figure 3). At other calibrated  
296 watersheds, the models perform similarly well with NSE varying between 0.45-0.60 for  
297 calibration period and 0.42-0.62 for validation period (Figures S1-S3). Simulated streamflow  
298 from the three models matches the in-situ measurements in both magnitudes and timing of  
299 hydrographs at event scales (Figure 3b). At annual scale, simulated annual peak flows are  
300 comparable to the observations in most years. However, in some years with extreme events, for  
301 example in January 1995, February 1998 and January 2005 (highlighted in Figure 3c), the  
302 simulated peaks are much lower than the gauge records. This disparity can be attributed to the  
303 input bias (e.g., precipitation or streamflow measurements). This was identified using an  
304 ‘extreme scenario’ simulation, which assumed 100% precipitation is transformed to surface  
305 runoff (i.e., without any loss due to, for example, infiltration or evapotranspiration) and  
306 transported immediately to river channels and represents the maximum streamflow considering  
307 groundwater is minimal in the study region (Beighley et al., 2003). Even in this extreme  
308 scenario, the simulated peaks were still lower (events highlighted in red in Figure 3c) or slightly  
309 higher (event highlighted in blue in Figure 3c) than the gauge observations. This is likely  
310 because that model forcings are biased low for these events. One possible source of this bias can  
311 be the grid-based precipitation dataset which averages the precipitation rates over the grid  
312 masking spatial heterogeneity and thus reducing precipitation rates at some locations. The  
313 uncertainties in gauge measurements can also be a bias source. For example, in typical  
314 conditions the uncertainty in streamflow measurements ranges between 6%-19% in small  
315 watersheds, but it can be higher during large storm events when accurate stage measurements are  
316 more difficult (Harmel et al., 2006). Beighley et al. (2003) also identified the overestimation of  
317 gauge records for the 1995 January event at Gauge 11119940. As for mean annual discharge, all

318 three models tend to overestimate it for the study period, mainly due to the overestimation of  
319 subsurface flow during dry seasons (Figure 3d). This highlights challenges of simulating  
320 hydrologic processes in semiarid regions under a Mediterranean climate.

321         Among the three hydrologic models, STP-HRR has the best overall performance (i.e.,  
322 highest average NSE), mainly due to its better ability for capturing flood peaks than the other  
323 two models (Figures 3, S1-S3). The peak performance is likely a result of the STP-HRR  
324 representing the runoff generation process as an exponential relationship between soil moisture  
325 and runoff rates, which makes runoff generation more sensitive to soil moisture dynamics as  
326 compared to the other two models. This algorithm is well suited to represent the significant  
327 nonlinearity of hydrologic response to rainfall in the study region. RCM-HRR and VIC-HRR  
328 have similar overall performance (i.e., similar average NSE), however, they represent hydrologic  
329 dynamics differently. VIC-HRR tends to perform better in representing small peak flows than  
330 RCM-HRR while worse in simulating mean flow (or total discharge volume) (Figures 3, S1-S3).  
331 This is because as the wet season proceeds, the lower soil layer is close to saturation (i.e.,  
332 relative soil moisture is higher than the threshold  $W_s$  for VIC-HRR) which initiate the quadratic  
333 relationship between soil moisture and subsurface runoff in VIC-HRR. This quadratic response  
334 to soil moisture conditions can lead to much higher subsurface runoff (1~2 orders of magnitude  
335 higher than that of RCM-HRR), which contributes to the lower performance in reproducing the  
336 total volume of discharge. This also explains that VIC-HRR generates the highest subsurface  
337 runoff during the wet season (Figure 4). In addition, VIC-HRR also generates the most surface  
338 runoff during wet season (Figure 4). This is because when soil is almost saturated, surface runoff  
339 in VIC-HRR is almost a linear function of precipitation with a coefficient of 1 (much larger than  
340 RCM-HRR which is 0.2 ( $C_2$ ) and STP-HRR which is around 0.5 depending on the watershed  
341 topography). The higher surface and subsurface runoff generated by VIC-HRR leads to the  
342 overestimation of mean annual flow (Figure 3d). However, there are no in-situ measurement of  
343 surface and subsurface runoff fluxes, and it is difficult to evaluate model performance for these  
344 quantities. In Figure 4, the simulated surface and subsurface runoff from National Land Data  
345 Assimilation Systems VIC model (NLDAS-VIC) (Xia et al., 2012) outputs are shown for the  
346 purpose of comparison. The NLDAS-VIC runoff simulations are from the same runoff  
347 generation model (i.e., VIC) as used in this work, and have similar spatial/temporal resolutions to

348 those in this study, which makes it a suitable reference for comparison. A similar pattern, i.e., a  
349 very high subsurface runoff, even higher than surface runoff, during wet season, can be found  
350 from NLDAS-VIC simulations. The surface runoff of NLDAS-VIC is lower than those  
351 generated by the models in this study, which is probably because of the difference in  
352 precipitation inputs. The NLDAS precipitation input is lower during wet season than that used in  
353 this study for the study region. In addition, the difference in spatial resolutions of precipitation  
354 ( $0.125^\circ$  for NLDAS vs.  $0.0625^\circ$  for this study) can also contribute to the difference in simulated  
355 runoff.

356         These results may suggest that STP-HRR is more suitable than VIC-HRR in representing  
357 hydrologic processes in Mediterranean regions where 80% annual precipitation is concentrated  
358 in a short period (roughly 3 months). As the wet season proceeds, the soil is close to saturation  
359 conditions, under which the saturation excess overland flow is dominant. That explains why  
360 STP-HRR performs best in this study region. VIC-HRR is probably more suitable to the regions  
361 where precipitation events are sparsely distributed where soil is not easy to get saturated.  
362 Although RCM is an empirical method, it performs fairly well in this study, mainly because it  
363 captures the nonlinearity of hydrologic processes through a switch between dry and wet surface  
364 runoff coefficients ( $C_1$  and  $C_2$ ) based on the soil moisture conditions.

365         Ten sets of parameters were selected for each model (Figure 5). Most optimal parameter  
366 sets (red circles in Figure 5) are very close, except for  $C_1$ ,  $K_{s\_all}$  in RCM-HRR and  $K_{s\_all}$ ,  $D_s$  in  
367 VIC-HRR, suggesting that most parameters are important factors controlling model performance.  
368 For the randomly selected parameters (green circles in Figure 5), most of them spread over the  
369 whole range, suggesting sufficient space for uncertainty analysis.

## 370 3.2 Impacts and Uncertainty analysis

371         The projected changes in monthly runoff (surface, subsurface and total) during 2081-  
372 2100 compared to 1986-2005 range between -100% and 300% (Figure 6a). The median changes  
373 indicate that surface runoff will probably increase in February and March, and decrease in other  
374 months (Figure 6a). This is because in the future, the onset of wet season will be delayed and  
375 more severe storm events will occur during the shorter wet season (mainly during February and  
376 March) (Feng et al., 2019). The decrease in subsurface runoff in all months is probably because

377 the decrease in the frequency (or total number) of storm events (Feng et al., 2019). The changes  
378 of monthly total runoff show similar pattern with the surface runoff, suggesting the more  
379 pronounced changes in surface runoff as compared to subsurface runoff. The major uncertainty  
380 sources are GCM and RCP, which account for ~45% of total uncertainty (Figure 6b). Hydrologic  
381 models contribute to ~10% of total uncertainty (Figure 6b). This suggests that the climate  
382 patterns (e.g., storm event frequency and intensity) are more important factors controlling the  
383 runoff generation than the hydrologic model algorithms.

384 For the 28 major watersheds in SBC, the projected changes in  $Q_m$  during 2081-2100 as  
385 compared to historical period 1986-2005, range from -100% to 220% (Figure S4). The median  
386 changes for each of these major watersheds are slightly above 0%, varying between 1% and 8%.  
387 The major uncertainty sources are GCM and RCP, which account for ~54% of the total  
388 uncertainty. Among the first order factors (i.e., GCM, RCP, hydrologic model and  
389 parameterization), hydrologic model ranks third after GCM and RCP, accounting for 10-15% of  
390 total uncertainty. In contrast, parameterization only induces less than 2% of the total uncertainty.  
391 The remaining 25-35% uncertainty is from the second, third and fourth order interactions  
392 between the four major sources. The projected relative changes in  $Q_p$  and  $Q_{100}$  are similar in  
393 magnitudes, both varying from -90% to 250% (Figure S5 and Figure 7). The median changes in  
394  $Q_p$  and  $Q_{100}$  for each watershed are higher than those of  $Q_m$ , ranging between 10-40%. For most  
395 of watersheds, GCM and RCP are the two major uncertainty contributors for  $Q_p$  and  $Q_{100}$ ,  
396 accounting for ~45% of total uncertainties. Hydrologic model contributes ~14% of total  
397 uncertainties in  $Q_p$  and  $Q_{100}$ . Compared to  $Q_m$ ,  $Q_p$  and  $Q_{100}$  get more uncertainty from the  
398 hydrologic models, which is likely due to highly nonlinear rainfall-runoff behavior and larger  
399 differences between runoff generation methods in generating peak flows as compared to average  
400 flow conditions.

401 Changes in  $Q_m$ ,  $Q_p$  and  $Q_{100}$  are higher under RCP 8.5, but the uncertainties are also  
402 higher (Figure 8), which suggests the higher contribution of RCP 8.5 in the uncertainties of  
403 higher-order interactions between RCP and other factors (i.e., GCM, hydrologic model and  
404 parameters). In Mission Creek watershed (USGS gauge No. 11119750), the probability of  
405 increase in  $Q_m$  under RCP 4.5 is only 51%. However, this probability increases to 64% under  
406 RCP 8.5. For the less frequent events ( $Q_p$  and  $Q_{100}$ ), the probabilities of positive changes are

407 higher: 78% and 85% for  $Q_p$  and  $Q_{100}$ , respectively, under RCP 8.5. This implies that if RCP 8.5  
408 happens in the future, the extreme events will probably get intensified.

409 Consistent with the work of Feng et al. (2019), this study suggests a delayed onset and  
410 shorter duration of wet season (Figure 9a). The median changes show that the wet season will  
411 start later by 3 days, and become shorter by ~6 days. The major uncertainty sources for both  
412 onset and duration of wet season are GCM (~20%) and hydrologic models (~15%). Different  
413 from discharge and runoff, the seasonality shows more uncertainty from hydrological models  
414 (15% vs 12%) and model parameters (~6% vs 2%) (Figure 9b). This is because the seasonality  
415 integrates the runoff generation, paths and transport processes for both surface and subsurface  
416 runoff, which are important for the timing and quantity of simulated discharge.

417 As the major carrier of nutrients/sediment, surface runoff and discharge are crucial for  
418 beach ecosystems in the study region (Myers et al., 2019;Aguilera and Melack, 2018). Nutrients  
419 and sediment build up over land surface and in channels during dry season, and get flushed with  
420 the initiation of wet season (Scott and Williams, 1978;Keller and Capelli, 1992;Bende-Michl et  
421 al., 2013;Aguilera and Melack, 2018). The nutrients/sediment fluxes are positively correlated  
422 with hydrologic variability, and the majority of them occurs at the beginning of the wet season  
423 (Aguilera and Melack, 2018;Homyak et al., 2014). Therefore, both timing and magnitude of  
424 runoff and discharge will impact the nutrients/sediment export to the coastal ecosystems. The  
425 findings in this study reveal that the surface runoff and river discharge (especially the extremes)  
426 will increase but get delayed during wet season (Figures 6 and 9), implying that the  
427 nutrients/sediment fluxes will likely increase and occur in a shorter and delayed period. The  
428 decrease in runoff (both surface and subsurface) during the dry season suggests that the soil  
429 moisture will be lower under future climate conditions in the study region. The longer and drier  
430 dry season will probably increase the occurrence of severe droughts and wildfires.

431 Compared to previous studies (e.g., Vetter et al. (2015), Schewe et al. (2014), Hagemann  
432 et al. (2013);Troin et al. (2018), and Asadieh and Krakauer (2017)), this work identifies  
433 relatively low uncertainty contributions from hydrologic models. The main reason for this is  
434 probably that the hydrologic model uncertainty in this study was only from runoff generation  
435 algorithms and associated parameters. As is, the three hydrologic models share common  
436 algorithms for ET and plane/channel routing, and the same model configuration (e.g., soil matrix

437 and model unit definition). These similarities among models likely reduced the differences in  
438 simulated runoff and discharge. In addition, the uniform calibration approach and parameter  
439 selection criteria were also likely to eliminate user/method bias which is common in studies that  
440 consider more than one hydrologic model. In contrast, the hydrologic models used in previous  
441 studies have their own model component algorithms (e.g., ET and routing algorithms), and  
442 model configurations. For example, the VIC model (here VIC refers to the original VIC model,  
443 and is different from the model used in this study; to clarify, in following text, VIC refers to the  
444 original VIC model while VIC-HRR refers to the model used in this study) applies an ET  
445 algorithm different from the one used in this study (Raoufi and Beighley, 2017), uses the grid-  
446 based model units ignoring the spatial arrangement, and has its own routing scheme which  
447 adopts the synthetic unit hydrograph concept. When comparing models owning their own  
448 component algorithms, the differences between models likely resulted in larger uncertainties in  
449 the simulation from hydrologic models in previous studies.

450 This study can also provide useful information for hydrologic model evaluation and  
451 selection. As discussed in section 3.1, the STP-HRR model is more suitable than the other two  
452 models for the study region, mainly due to its ability to represent the highly non-linear  
453 hydrological response to precipitation forcings. This implies hydrologic models adopting the  
454 saturation excess runoff generation algorithms may be more suitable for areas with a  
455 Mediterranean climate. The uncertainties from hydrologic models are larger than those from the  
456 hydrologic model parameters for all variables (i.e., discharge, runoff and seasonality), suggesting  
457 the inter-model variability is larger than the intra-model variability (from model parameters).  
458 This implies that model selection is more important than the parameter selection, and that the  
459 parameter equifinality (or non-uniqueness) is less of a concern when quantifying climate change  
460 impacts on hydrologic fluxes using an ensemble of GCM forcings. In this study, only the runoff  
461 generation algorithm was investigated. Other hydrologic model components, such as ET  
462 algorithms and routing methods, also have variants. The choice of these components may also  
463 make a difference in the total uncertainties in simulated runoff and streamflow. In addition, the  
464 methods for GCM downscaling can also contribute to the uncertainty in predicted changes in  
465 hydrology. Further study integrating different algorithms for hydrologic model components as  
466 well as GCM downscaling methods can be conducted in the future. Such analysis can be useful



467 to guide stakeholders to select appropriate hydrologic algorithms and to develop actionable  
468 adaptation and mitigation strategies to accommodate climate change.

469 This is the first study investigating hydrologic model uncertainty solely from runoff  
470 generation algorithms for a region with the Mediterranean climate. The framework developed in  
471 this study can be potentially used to identify the internal uncertainties of hydrologic models, i.e.,  
472 uncertainties from hydrologic model components (e.g., runoff generation algorithms, ET  
473 algorithms and routing models), which is particularly important for assessing model performance  
474 and quantifying the relative roles of different components in the uncertainty of simulations. This  
475 study region is a representative Mediterranean area characterized by dry summers and wet  
476 winters. This climate pattern and the highly non-linear relationship between climate and  
477 hydrology significantly impact local society, agriculture and ecosystems as discussed before. The  
478 findings in this study including the favorability of STP algorithm, the important role of GCM  
479 selection and the negligible role of hydrologic model parameters in the uncertainty, can be useful  
480 for studies associated with hydrologic model evaluation and climate change impact analysis for  
481 other Mediterranean regions.

## 482 **4. Conclusions**

483 A modeling framework which integrates multiple runoff generation algorithms (VIC,  
484 STP and RCM) with the HRR routing model was developed. Forced with an ensemble of GCM  
485 outputs under different emission scenarios, this framework is able to quantify the climate change  
486 impacts on surface and subsurface runoff, streamflow and hydrologic seasonality, and evaluate  
487 the associated uncertainties from different sources (i.e., RCPs, GCMs, hydrologic process  
488 models and parameterization). The results show that the surface runoff will likely increase in  
489 February and March, while decrease in other months, and the subsurface runoff will likely  
490 decrease due to changes in the patterns of storm events. The median changes in mean annual  
491 discharge for the major watersheds in SBC are 1-8%, with an uncertainty of 320% (here,  
492 uncertainty refers to the range of predicted relative changes among models, that is, from -100%  
493 to +220%); the median changes in annual peak discharge and 100-yr flood discharge are higher  
494 than those of mean annual discharge, varying between 10% and 40%, but with a higher  
495 uncertainty of 340% (-90% to +250%). The results based on the BMA analysis indicate that there

496 is a high probability (up to 85%) that streamflow, especially the extreme quantities (e.g.,  $Q_{100}$ )  
497 under RCP 8.5, will increase. The seasonality analysis shows that the wet season will be delayed  
498 (by 3 days, median) and shortened (by 6 days, median). For the uncertainties in the projected  
499 changes in runoff and discharge, GCM and RCP are the top two contributors, accounting for  
500 roughly 50% of total uncertainties at most major watersheds in SBC, while hydrologic process  
501 models (i.e., runoff generation modules) contribute ~12% on average with the remaining 30-40%  
502 of the uncertainty coming from the interactions between these individual sources. Hydrologic  
503 model parameters alone contribute less than 2% of the uncertainty. In contrast, for the changes in  
504 seasonality, the uncertainty contributions from hydrologic models (~15%) and hydrologic model  
505 parameters (~6%) are higher as compared to those for runoff and discharge, making GCMs and  
506 hydrologic models the two major uncertainty sources.

507         Unique to the framework in this study, the uncertainties from different hydrologic model  
508 components (e.g., runoff generation process) and associated model parameterizations can be  
509 identified and quantified. The results can be useful for practices and studies in many fields, e.g.,  
510 water resources, risk controls and ecosystem conservation, for the study region as well as other  
511 Mediterranean regions.

## 512 **Code availability**

513         The source code supporting this work is available on Github:  
514 <https://github.com/dongmeifeng-2019/HydroUncertainty>

## 515 **Author contribution**

516 D. Feng designed the experiments, developed the models, performed the simulations, and prepared  
517 the manuscript. E. Beighley conceptualized the project, and reviewed the manuscript.

## 518 **Competing interests**

519 The authors declare that they have no conflict of interest.

## 520 **Acknowledgments**

521         This research was supported by the Santa Barbara Area Coastal Ecosystem Vulnerability  
522 Assessment (SBA CEVA) with funding from the NOAA Climate Program Office Coastal and

523 Ocean Climate Applications (COCA) and Sea Grant Community Climate Adaptation Initiative  
524 (CCAI), and the National Science Foundation's Long-Term Ecological Research (LTER) program  
525 (Santa Barbara Coastal LTER - OCE9982105, OCE-0620276 and OCE-123277). The authors  
526 thank Dr. David Hadka at Pennsylvania State University and Chinedum Eluwa at University of  
527 Massachusetts, Amherst, for their help with setting up the Borg MOEA. The authors acknowledge  
528 two anonymous reviewers and Dr. Konstantinos Andreadis for their valuable comments that  
529 significantly improved the manuscript.

530 **References:**

- 531 Addor, N., Rössler, O., Köplin, N., Huss, M., Weingartner, R., and Seibert, J.: Robust changes and  
532 sources of uncertainty in the projected hydrological regimes of Swiss catchments, *Water*  
533 *Resources Research*, 50, 7541-7562, 10.1002/2014wr015549, 2014.
- 534 Aguilera, R., and Melack, J. M.: Relationships Among Nutrient and Sediment Fluxes, Hydrological  
535 Variability, Fire, and Land Cover in Coastal California Catchments, *Journal of Geophysical Research:*  
536 *Biogeosciences*, 123, 2568-2589, doi:10.1029/2017JG004119, 2018.
- 537 Alder, J. R., and Hostetler, S. W.: The Dependence of Hydroclimate Projections in Snow-Dominated  
538 Regions of the Western United States on the Choice of Statistically Downscaled Climate Data,  
539 *Water Resources Research*, 55, 2279-2300, 10.1029/2018WR023458, 2019.
- 540 Asadieh, B., and Krakauer, N. Y.: Global change in streamflow extremes under climate change over  
541 the 21st century, *Hydrology and Earth System Sciences*, 21, 5863, 2017.
- 542 Barnett, T. P., Adam, J. C., and Lettenmaier, D. P.: Potential impacts of a warming climate on water  
543 availability in snow-dominated regions, *Nature*, 438, 303-309, 2005.
- 544 Beighley, E., Eggert, K. G., Dunne, T., He, Y., Gummadi, V., and Verdin, K. L.: Simulating hydrologic  
545 and hydraulic processes throughout the Amazon River Basin, *Hydrological Processes*, 23, 1221-  
546 1235, 10.1002/hyp.7252, 2009.
- 547 Beighley, R. E., Melack, J. M., and Dunne, T.: Impacts of California's climatic regimes and coastal  
548 land use change on streamflow characteristics, *JAWRA Journal of the American Water Resources*  
549 *Association*, 39, 1419-1433, 10.1111/j.1752-1688.2003.tb04428.x, 2003.
- 550 Bende-Michl, U., Verburg, K., and Cresswell, H. P.: High-frequency nutrient monitoring to infer  
551 seasonal patterns in catchment source availability, mobilisation and delivery, *Environmental*  
552 *Monitoring and Assessment*, 185, 9191-9219, 10.1007/s10661-013-3246-8, 2013.
- 553 Beven, K., R. Lamb, P. Quinn, R. Romanowicz, and Freer, J.: *Topmodel, Computer Models of*  
554 *Watershed Hydrology*, edited by: Singh, V. P., Water Resources Publications, Highlands Ranch,  
555 Colorado, 1995.
- 556 Beven, K.: *Rainfall-Runoff Modelling: The Primer*, John Wiley, Chichester, 2000.
- 557 Beven, K. J., and Cloke, H. L.: Comment on “Hyperresolution global land surface modeling:  
558 Meeting a grand challenge for monitoring Earth's terrestrial water” by Eric F. Wood et al, *Water*  
559 *Resources Research*, 48, 2012.
- 560 Cai, W., Borlace, S., Lengaigne, M., van Rensch, P., Collins, M., Vecchi, G., Timmermann, A.,

561 Santoso, A., McPhaden, M. J., Wu, L., England, M. H., Wang, G., Guilyardi, E., and Jin, F.-F.:  
562 Increasing frequency of extreme El Nino events due to greenhouse warming, *Nature Clim. Change*,  
563 4, 111-116, 10.1038/nclimate2100, 2014.

564 Chegwiddden, O. S., Nijssen, B., Rupp, D. E., Arnold, J. R., Clark, M. P., Hamman, J. J., Kao, S.-C.,  
565 Mao, Y., Mizukami, N., Mote, P. W., Pan, M., Pytlak, E., and Xiao, M.: How Do Modeling Decisions  
566 Affect the Spread Among Hydrologic Climate Change Projections? Exploring a Large Ensemble of  
567 Simulations Across a Diversity of Hydroclimates, *Earth's Future*, 7, 623-637,  
568 10.1029/2018ef001047, 2019.

569 Dai, A.: The influence of the inter-decadal Pacific oscillation on US precipitation during 1923–2010,  
570 *Climate dynamics*, 41, 633-646, 2013.

571 Dettinger, M.: Climate change, atmospheric rivers, and floods in California - a multimodel analysis  
572 of storm frequency and magnitude changes, *Journal of the American Water Resources*  
573 *Association*, 47, 514-523, 10.1111/j.1752-1688.2011.00546.x, 2011.

574 Duan, Q., Ajami, N. K., Gao, X., and Sorooshian, S.: Multi-model ensemble hydrologic prediction  
575 using Bayesian model averaging, *Advances in Water Resources*, 30, 1371-1386,  
576 <https://doi.org/10.1016/j.advwatres.2006.11.014>, 2007.

577 Eisner, S., Flörke, M., Chamorro, A., Daggupati, P., Donnelly, C., Huang, J., Hundecha, Y., Koch, H.,  
578 Kalugin, A., Krylenko, I., Mishra, V., Piniewski, M., Samaniego, L., Seidou, O., Wallner, M., and  
579 Krysanova, V.: An ensemble analysis of climate change impacts on streamflow seasonality across  
580 11 large river basins, *Climatic Change*, 141, 401-417, 10.1007/s10584-016-1844-5, 2017.

581 Feng, D., Beighley, E., Hughes, R., and Kimbro, D.: Spatial and temporal variations in eastern U.S.  
582 Hydrology: Responses to global climate variability, *JAWRA Journal of the American Water*  
583 *Resources Association*, 52, 1089-1108, 10.1111/1752-1688.12445, 2016.

584 Feng, D., Beighley, E., Raoufi, R., Melack, J., Zhao, Y., Iacobellis, S., and Cayan, D.: Propagation of  
585 future climate conditions into hydrologic response from coastal southern California watersheds,  
586 *Climatic Change*, 153, 199-218, 10.1007/s10584-019-02371-3, 2019.

587 Giuntoli, I., Villarini, G., Prudhomme, C., and Hannah, D. M.: Uncertainties in projected runoff  
588 over the conterminous United States, *Climatic Change*, 150, 149-162, 10.1007/s10584-018-2280-  
589 5, 2018.

590 Hadka, D., and Reed, P.: Borg: An auto-adaptive many-objective evolutionary computing  
591 framework, *Evolutionary computation*, 21, 231-259, 2013.

592 Hagemann, S., Chen, C., Clark, D. B., Folwell, S., Gosling, S. N., Haddeland, I., Hanasaki, N., Heinke,  
593 J., Ludwig, F., Voss, F., and Wiltshire, A. J.: Climate change impact on available water resources  
594 obtained using multiple global climate and hydrology models, *Earth Syst. Dynam.*, 4, 10.5194/esd-

595 4-129-2013, 2013.

596 Harmel, R. D., Cooper, R. J., Slade, R. M., Haney, R. L., and Arnold, J. G.: Cumulative uncertainty in  
597 measured streamflow and water quality data for small watersheds, Transactions of the ASABE,  
598 49, 689-701, 2006.

599 Hattermann, F. F., Vetter, T., Breuer, L., Su, B., Daggupati, P., Donnelly, C., Fekete, B., Flörke, F.,  
600 Gosling, S. N., Hoffmann, P., Liersch, S., Masaki, Y., Motovilov, Y., Müller, C., Samaniego, L., Stacke,  
601 T., Wada, Y., Yang, T., and Krysnova, V.: Sources of uncertainty in hydrological climate impact  
602 assessment: a cross-scale study, Environmental Research Letters, 13, 015006, 10.1088/1748-  
603 9326/aa9938, 2018.

604 Homyak, P. M., Sickman, J. O., Miller, A. E., Melack, J. M., Meixner, T., and Schimel, J. P.: Assessing  
605 Nitrogen-Saturation in a Seasonally Dry Chaparral Watershed: Limitations of Traditional Indicators  
606 of N-Saturation, Ecosystems, 17, 1286-1305, 10.1007/s10021-014-9792-2, 2014.

607 Horton, R. E.: The Rôle of infiltration in the hydrologic cycle, Eos, Transactions American  
608 Geophysical Union, 14, 446-460, 10.1029/TR014i001p00446, 1933.

609 Kay, A. L., Davies, H. N., Bell, V. A., and Jones, R. G.: Comparison of uncertainty sources for climate  
610 change impacts: flood frequency in England, Climatic Change, 92, 41-63, 10.1007/s10584-008-  
611 9471-4, 2009.

612 Keller, E. A., and Capelli, M. H.: VENTURA RIVER FLOOD OF FEBRUARY 1992: A LESSON IGNORED?,  
613 JAWRA Journal of the American Water Resources Association, 28, 813-832, 10.1111/j.1752-  
614 1688.1992.tb03184.x, 1992.

615 Liang, X., Wood, E. F., and Lettenmaier, D. P.: Surface soil moisture parameterization of the VIC-2L  
616 model: Evaluation and modification, Global and Planetary Change, 13, 195-206,  
617 [https://doi.org/10.1016/0921-8181\(95\)00046-1](https://doi.org/10.1016/0921-8181(95)00046-1), 1996.

618 Livneh, B., Bohn, T. J., Pierce, D. W., Munoz-Arriola, F., Nijssen, B., Vose, R., Cayan, D. R., and Brekke,  
619 L.: A spatially comprehensive, hydrometeorological data set for Mexico, the U.S., and Southern  
620 Canada 1950–2013, Scientific Data, 2, 150042, 10.1038/sdata.2015.42, 2015.

621 Milly, P. C. D., Dunne, K. A., and Vecchia, A. V.: Global pattern of trends in streamflow and water  
622 availability in a changing climate, Nature, 438, 347-350, 2005.

623 Myers, M. R., Barnard, P. L., Beighley, E., Cayan, D. R., Dugan, J. E., Feng, D., Hubbard, D. M.,  
624 Iacobellis, S. F., Melack, J. M., and Page, H. M.: A multidisciplinary coastal vulnerability assessment  
625 for local government focused on ecosystems, Santa Barbara area, California, Ocean & Coastal  
626 Management, 104921, <https://doi.org/10.1016/j.ocecoaman.2019.104921>, 2019.

627 Niu, G. Y., Yang, Z. L., Dickinson, R. E., and Gulden, L. E.: A simple TOPMODEL-based runoff

628 parameterization (SIMTOP) for use in global climate models, *Journal of Geophysical Research:*  
629 *Atmospheres*, 110, doi:10.1029/2005JD006111, 2005.

630 Pierce, D. W., Cayan, D. R., and Thrasher, B. L.: Statistical downscaling using localized constructed  
631 analogs (LOCA), *Journal of Hydrometeorology*, 15, 2558-2585, 2014.

632 Pierce, D. W., Cayan, D. R., Maurer, E. P., Abatzoglou, J. T., and Hegewisch, K. C.: Improved Bias  
633 Correction Techniques for Hydrological Simulations of Climate Change, *Journal of*  
634 *Hydrometeorology*, 16, 2421-2442, 10.1175/jhm-d-14-0236.1, 2015.

635 Pierce, D. W., Kalansky, J. F., and Cayan, D. R.: Climate, drought, and sea level rise scenarios for  
636 California's fourth climate change assessment. , California Energy Commission and California  
637 Natural Resources Agency, 2018.

638 Raoufi, R., and Beighley, E.: Estimating daily global evapotranspiration using penman–monteith  
639 equation and remotely sensed land surface temperature, *Remote Sensing*, 9, 1138, 2017.

640 Schewe, J., Heinke, J., Gerten, D., Haddeland, I., Arnell, N. W., Clark, D. B., Dankers, R., Eisner, S.,  
641 Fekete, B. M., Colón-González, F. J., Gosling, S. N., Kim, H., Liu, X., Masaki, Y., Portmann, F. T., Satoh,  
642 Y., Stacke, T., Tang, Q., Wada, Y., Wisser, D., Albrecht, T., Frieler, K., Piontek, F., Warszawski, L., and  
643 Kabat, P.: Multimodel assessment of water scarcity under climate change, *Proceedings of the*  
644 *National Academy of Sciences*, 111, 3245-3250, 10.1073/pnas.1222460110, 2014.

645 Scott, K. M., and Williams, R. P.: Erosion and sediment yields in the Transverse Ranges, southern  
646 California, 38 p., 1978.

647 Su, B., Huang, J., Zeng, X., Gao, C., and Jiang, T.: Impacts of climate change on streamflow in the  
648 upper Yangtze River basin, *Climatic Change*, 141, 533-546, 10.1007/s10584-016-1852-5, 2017.

649 Tao, H., Gemmer, M., Bai, Y., Su, B., and Mao, W.: Trends of streamflow in the Tarim River Basin  
650 during the past 50years: Human impact or climate change?, *Journal of hydrology*, 400, 1-9, 2011.

651 Troin, M., Arsenault, R., Martel, J.-L., and Brissette, F.: Uncertainty of Hydrological Model  
652 Components in Climate Change Studies over Two Nordic Quebec Catchments, *Journal of*  
653 *Hydrometeorology*, 19, 27-46, 10.1175/jhm-d-17-0002.1, 2018.

654 Valentina, K., Tobias, V., Stephanie, E., Shaochun, H., Ilias, P., Michael, S., Alexander, G., Rohini, K.,  
655 Valentin, A., Berit, A., Alejandro, C., Ann van, G., Dipangkar, K., Anastasia, L., Vimal, M., Stefan, P.,  
656 Julia, R., Ousmane, S., Xiaoyan, W., Michel, W., Xiaofan, Z., and Fred, F. H.: Intercomparison of  
657 regional-scale hydrological models and climate change impacts projected for 12 large river basins  
658 worldwide—a synthesis, *Environmental Research Letters*, 12, 105002, 2017.

659 Vetter, T., Huang, S., Aich, V., Yang, T., Wang, X., Krysanova, V., and Hattermann, F.: Multi-model  
660 climate impact assessment and intercomparison for three large-scale river basins on three

661 continents, *Earth System Dynamics*, 6, 17, 2015.

662 Vicky, E., E., W. D., Bin, G., A., L. D., and Martin, R. F.: Global Analysis of Climate Change Projection  
663 Effects on Atmospheric Rivers, *Geophysical Research Letters*, 45, 4299-4308,  
664 doi:10.1029/2017GL076968, 2018.

665 Vidal, J.-P., Hingray, B., Magand, C., Sauquet, E., and Ducharne, A.: Hierarchy of climate and  
666 hydrological uncertainties in transient low-flow projections, *Hydrology and Earth System Sciences*,  
667 20, 3651, 2016.

668 Wilby, R. L., and Harris, I.: A framework for assessing uncertainties in climate change impacts:  
669 Low-flow scenarios for the River Thames, UK, *Water Resources Research*, 42,  
670 doi:10.1029/2005WR004065, 2006.

671 Wood, E. F., Lettenmaier, D. P., and Zartarian, V. G.: A land-surface hydrology parameterization  
672 with subgrid variability for general circulation models, *Journal of Geophysical Research:*  
673 *Atmospheres*, 97, 2717-2728, 10.1029/91JD01786, 1992.

674 Xia, Y., et al.: NLDAS VIC Land Surface Model L4 Monthly 0.125 x 0.125 degree, version 002,  
675 Goddard Earth Sciences Data and Information Services Center (GES DISC), NASA/GSFC/HSL,  
676 Greenbelt, Maryland, USA, 2012.

677 Yamazaki, D., Ikeshima, D., Tawatari, R., Yamaguchi, T., O'Loughlin, F., Neal, J. C., Sampson, C. C.,  
678 Kanae, S., and Bates, P. D.: A high-accuracy map of global terrain elevations, *Geophysical Research*  
679 *Letters*, 44, 5844-5853, 10.1002/2017gl072874, 2017.

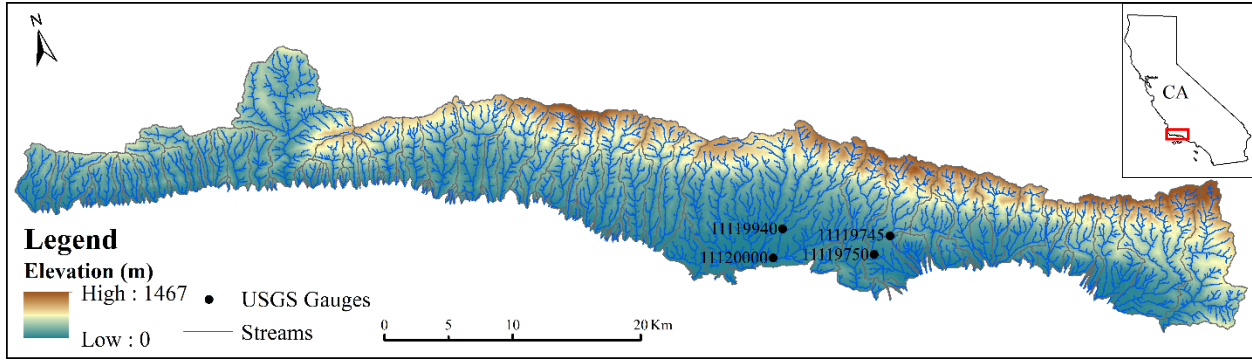
680

681

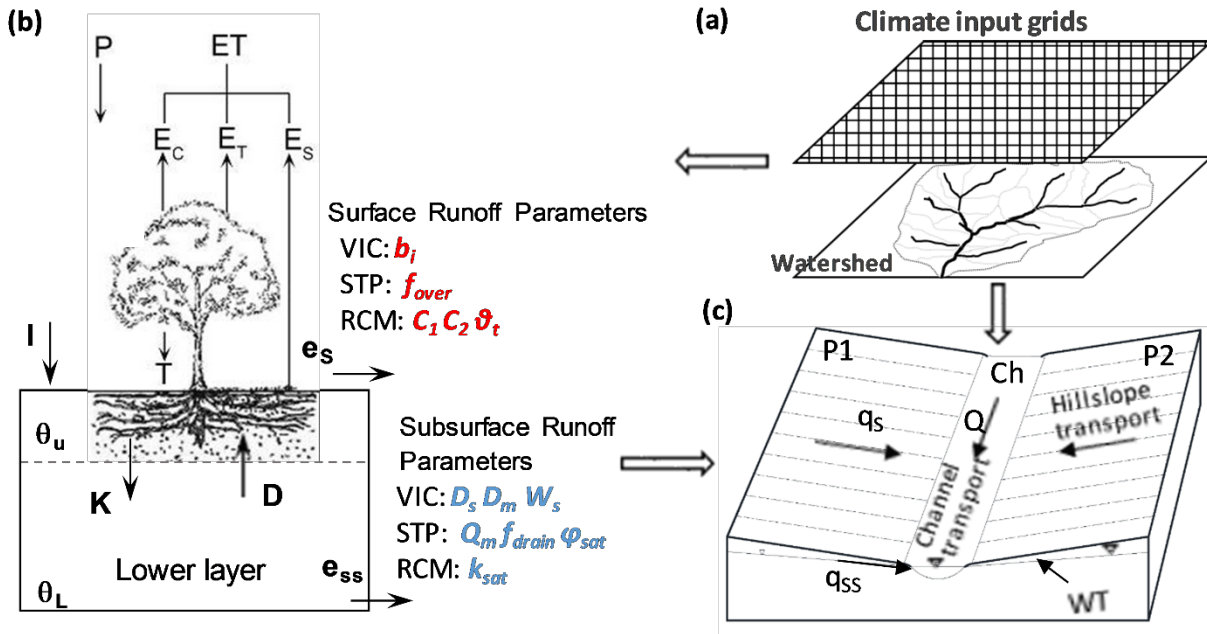


682 **Table 1:** Calibrated parameters for hydrologic models

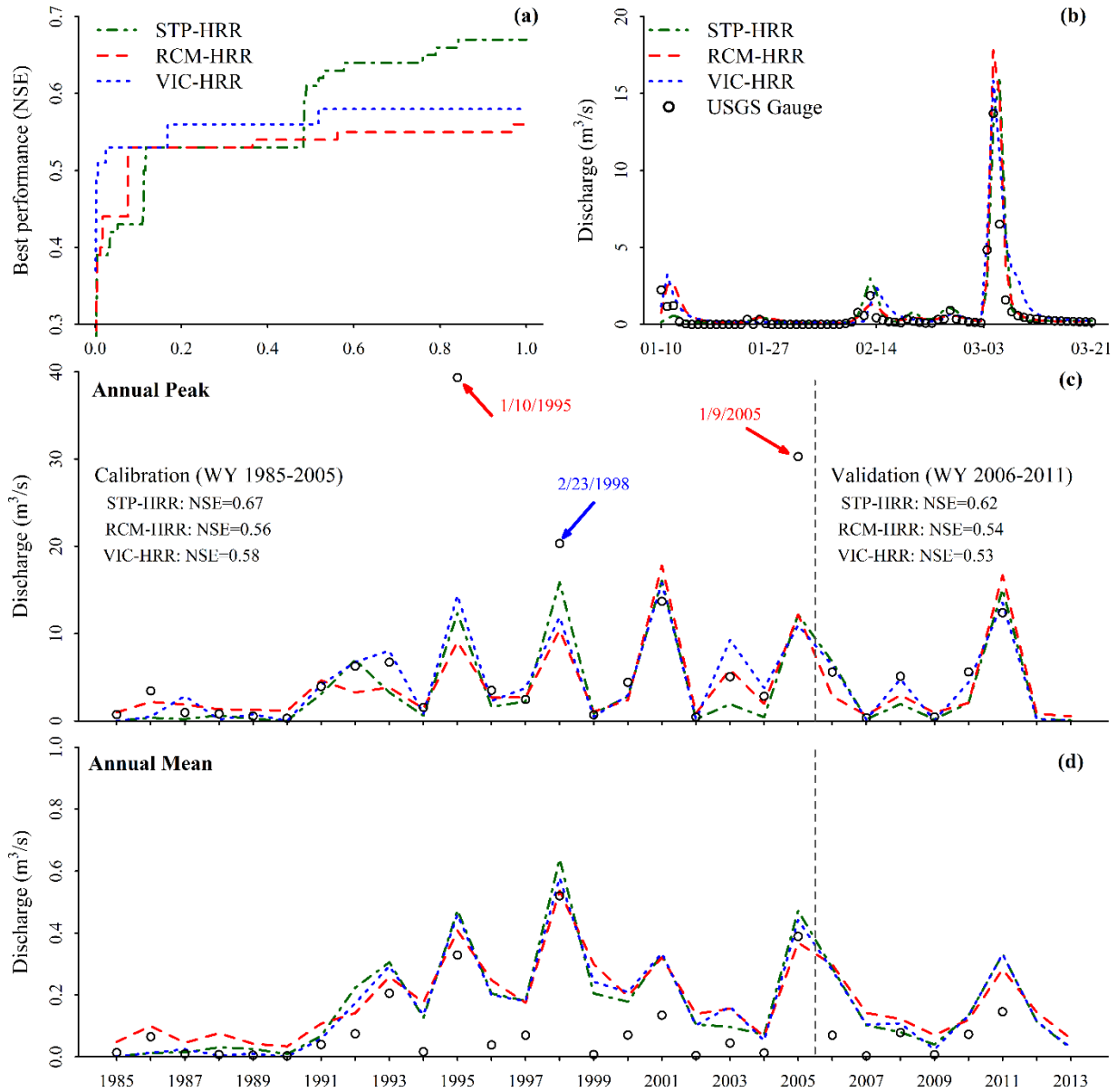
Parameters	Description	Unit	Range	RCM-HRR	VIC-HRR	STP-HRR
$K_{s\_all}$	coefficient to adjust surface roughness	-	1-20	✓	✓	✓
$K_{ss\_all}$	coefficient to adjust horizontal hydraulic conductivity	-	10-200	✓	✓	✓
$K_{sat\_all}$	coefficient to adjust vertical hydraulic conductivity	-	0.01-5.0	✓		
$C_1$	dry runoff coefficient	-	0-0.3	✓		
$C_2$	wet runoff coefficient	-	0.2-0.8	✓		
$\theta_t$	soil moisture threshold separating dry and wet conditions	-	0.2-0.8	✓		
$b_{in}$	Infiltration curve shape parameter	-	0.005-0.5		✓	
$D_m$	maximum baseflow	$m \cdot d^{-1}$	0 -0.037		✓	
$D_s$	fraction of $D_M$ where non-linear baseflow begins	-	0 -0.005		✓	
$W_s$	fraction of the maximum soil moisture where non-linear baseflow occurs	-	0.92-1.0		✓	
$f_{over}$	Surface runoff coefficient	$m^{-1}$	0.1-5			✓
$f_{drain}$	Subsurface runoff coefficient	$m^{-1}$	0.1-5			✓
$Q_m$	maximum baseflow	$m \cdot d^{-1}$	0.864-1728			✓
$\varphi_{sat}$	Saturated suction head in the soil	m	-3.05-0			✓



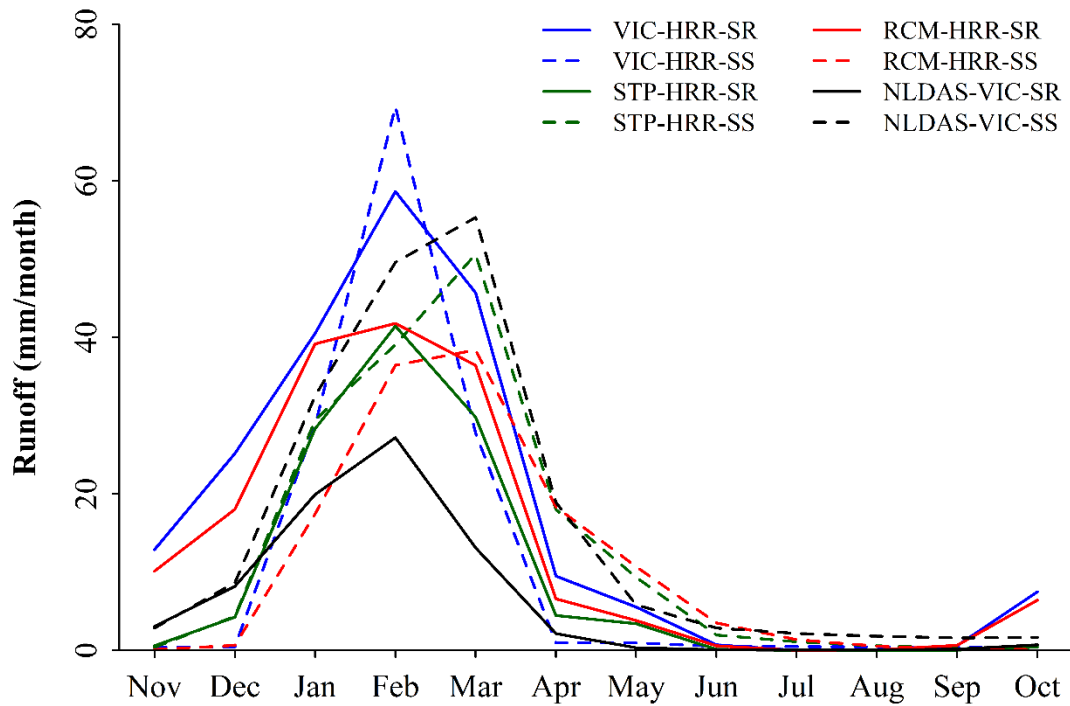
683 **Figure 1:** Study region with USGS streamflow gauges. The inset figure indicates the location of  
 684 SBC in the state of California (CA).



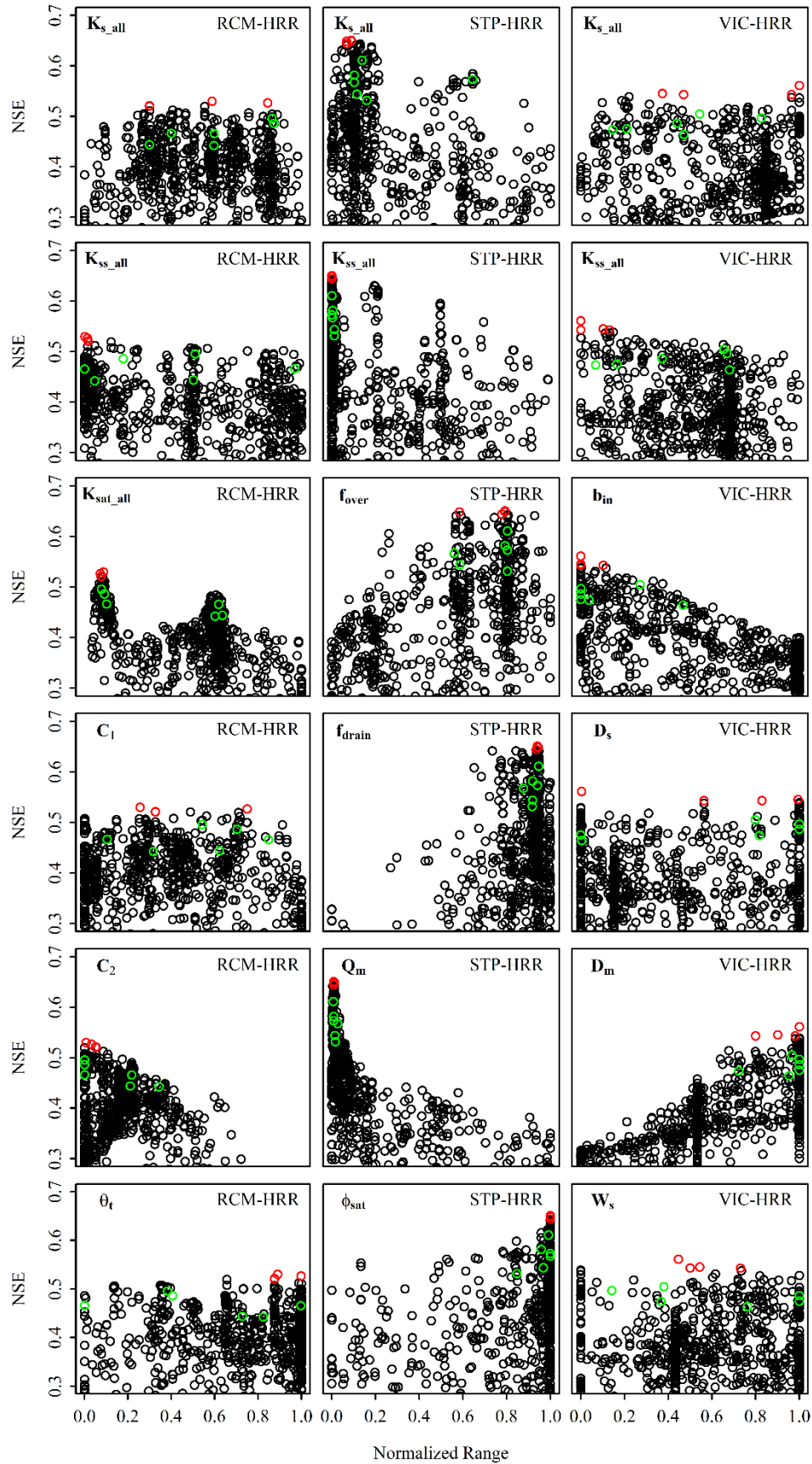
685  
 686 **Figure 2:** The conceptual framework about the hydrologic models used in this study. Portions of  
 687 this figure were adapted from the work of Beighley et al. (2009). (a) shows the grid-based climate  
 688 inputs for hydrologic models; (b) shows water balance models; P is precipitation; ET is  
 689 evapotranspiration;  $E_s$  is soil evaporation;  $E_c$  is canopy evaporation;  $E_T$  is transpiration;  $e_s$  is water  
 690 available for surface runoff;  $e_{ss}$  is water available for subsurface runoff;  $\theta_u$  is relative soil moisture  
 691 in upper soil layer;  $\theta_L$  is relative soil moisture in lower soil layer; I is infiltration; K is water flux  
 692 from the upper layer to the lower layer; and D is diffusive water flux from the lower layer to the  
 693 upper layer; and (c) shows HRR routing model; the “open-book” assumption: two identical planes  
 694 (P1 and P2) with the channel (Ch) in the center of each sub-basin;  $q_s$  is the surface runoff;  $q_{ss}$  is  
 695 subsurface runoff; Q is discharge in the river channel, and WT is groundwater table. The  
 696 parameters in red italic are for surface runoff generation, the parameters in blue italic are for  
 697 subsurface runoff generation. The first columns in the tables indicate the models that the  
 698 parameters are used for. The definition of these parameters can be found in the supporting  
 699 information.



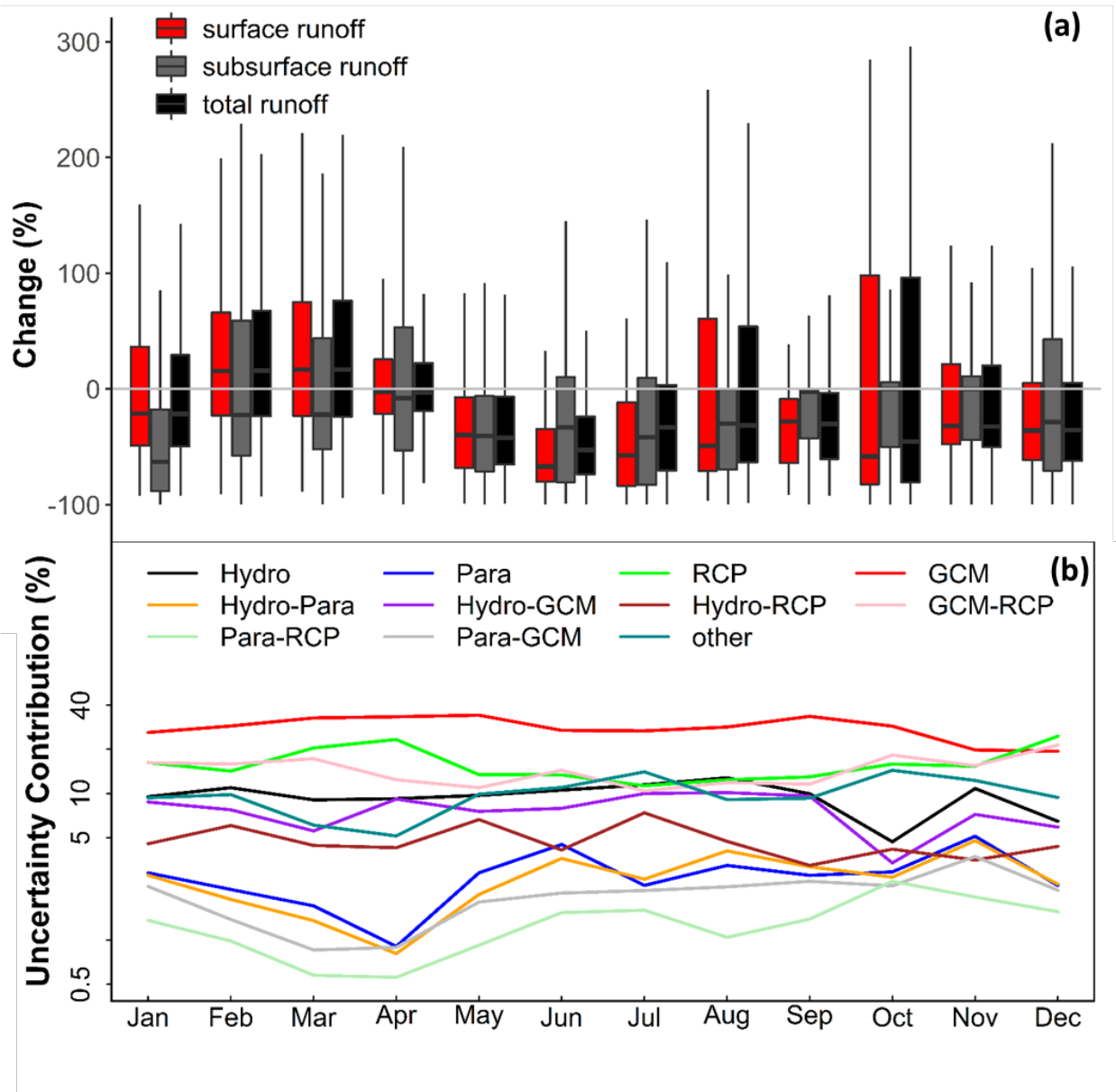
700 **Figure 3:** Model performance for calibration and validation periods: (a) model performance (assessed by  
701 NSE) during calibration process, the x axis is the normalized calibration process; the “normalized  
702 calibration process” means the x axis range is normalized by the number of iterations during calibration;  
703 (b) hydrographs simulated by three calibrated models and measured by the USGS gauge; in order to show  
704 the details of the hydrographs, they are zoomed in to the wet season in 2001; the model performance is  
705 similar in other years; (c) simulated annual peak flow during calibration (water year 1985-2005) and  
706 validation (water year 2006-2011) periods as compared with in situ observations; black texts indicate model  
707 performance (i.e., NSE); the points highlighted in red arrows indicate the events were not reproduced by  
708 models due to the input (e.g., precipitation or discharge observation) bias; the point highlighted in blue  
709 arrow is similar to those in red but at a lower probability; and (d) simulated and observed annual mean flow  
710 during calibration and validation periods. For clarity, only results for the Mission Creek watershed (USGS  
711 gauge NO. 11119750) are shown here; results for other gauged watersheds are similar and can be found in  
712 the Supporting Information (Figure S1-S3).



713 **Figure 4:** Simulated monthly surface and subsurface runoff for the Mission Creek watershed (USGS  
 714 gauge NO. 11119750) by three models for the calibration period (water year 1985-2005). Surface runoff  
 715 is denoted by 'SR' and subsurface runoff is denoted by 'SS' in this figure. Monthly surface and  
 716 subsurface runoff from National Land Data Assimilation Systems (NLDAS) VIC model simulation for  
 717 the same period are shown here for comparison purpose.

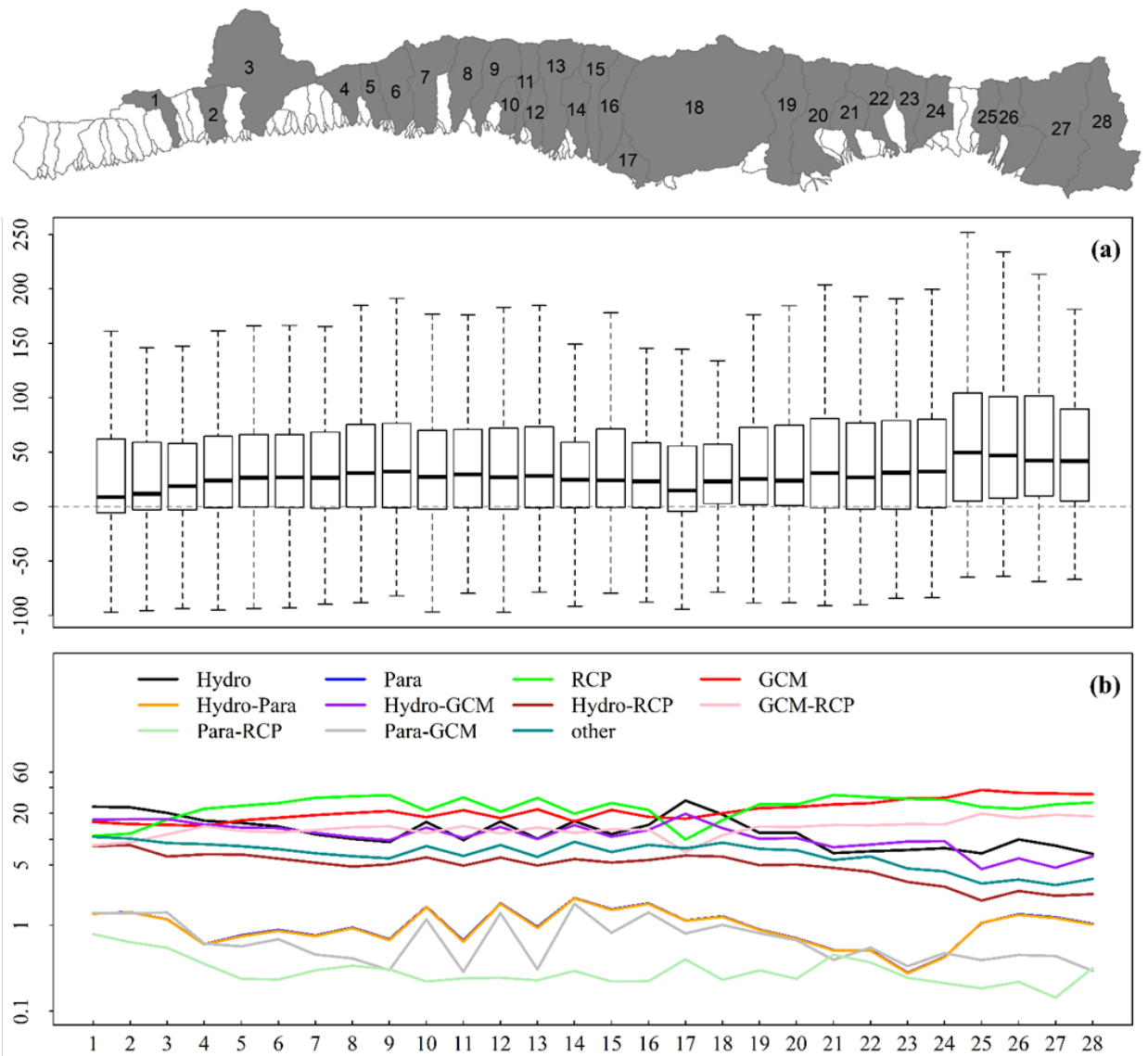


719 **Figure 5:** Parameters (black circles) sampled during calibration process and their corresponding  
720 performance (assessed by NSE). The red circles indicate the 4 parameter sets with highest NSE  
721 values, and the green circles indicate 6 randomly selected parameter sets from the top 20%  
722 samples (ranked by NSE). These ten parameter sets were used for uncertainty analysis. In this  
723 figure, the parameter values are normalized by their ranges (shown in Table 1), so the range of  
724 the x axis is 0-1. The parameters were sampled throughout their whole ranges, however, for  
725 clarity, samples with NSE lower than 0.3 are not shown in this figure.

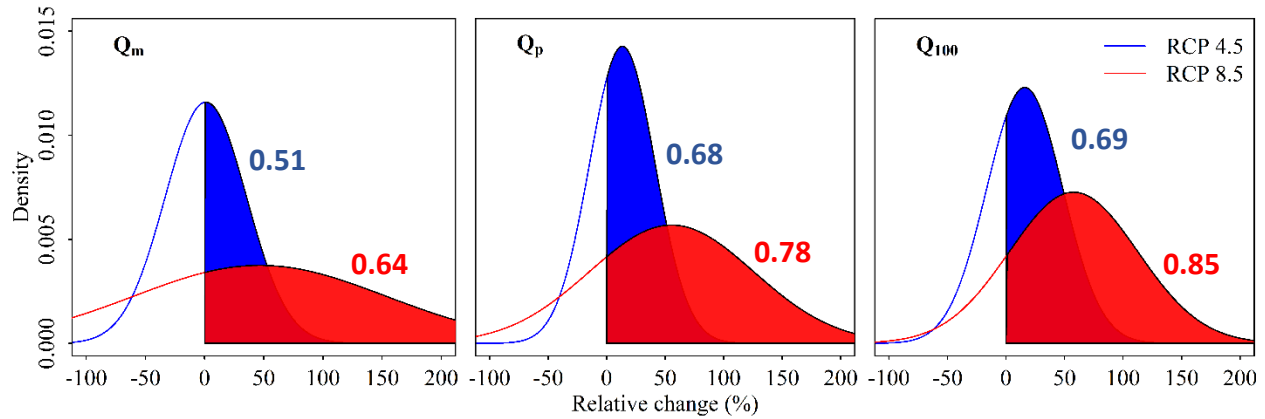


726 **Figure 6: (a)** Projected relative changes (%) in monthly surface runoff, subsurface runoff and total  
727 runoff in the whole study region during 2081-2100 as compared to historical period (1986-2005);  
728 **(b)** Relative contributions (%) of the uncertainties for the projected changes in the monthly total  
729 runoff; Hydro = Hydrologic models; Para = hydrologic model parameters; GCM = General  
730 Circulation Models; RCP = Representative concentration pathways (emission scenarios); “other”  
731 is the uncertainty from the 3<sup>rd</sup> and 4<sup>th</sup> orders of interactions between the 4 major sources (i.e.,  
732 GCMs, RCPs, Hydrologic models and parameters).

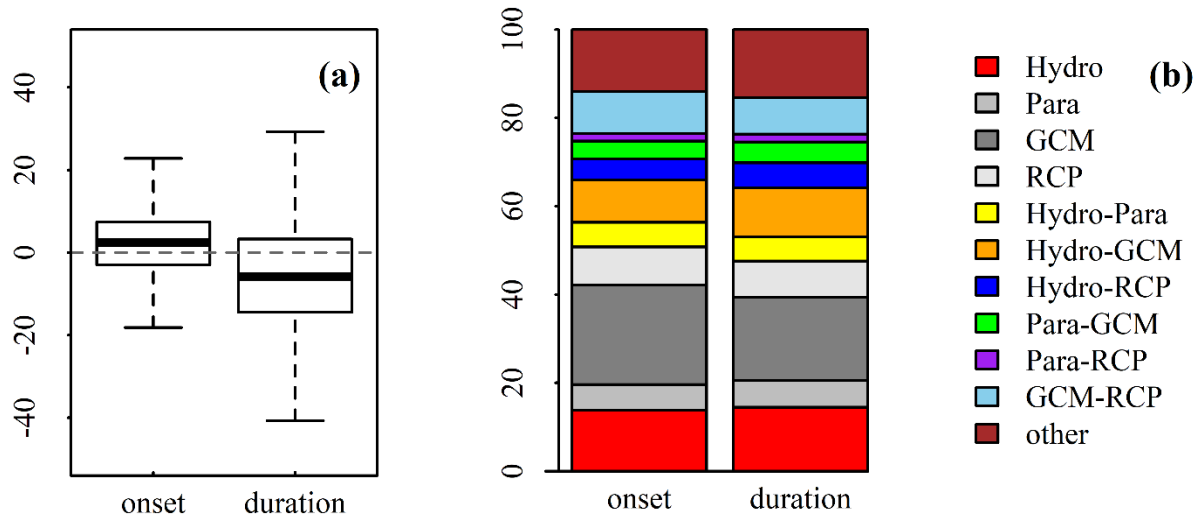




733 **Figure 7: (a)** Projected relative changes (%) in 100-yr flood discharge ( $Q_{100}$ ) in the major SBC  
 734 watersheds (indicated by the grey watersheds in the map) during 2081-2100 as compared to  
 735 historical period (1986-2005); each bar depicts relative changes in minimum, maximum, median,  
 736 1st and 3rd quartiles for the ensemble outputs; bars from left to right spatially corresponding to  
 737 watersheds from west to east. For clarity, only watersheds with drainage areas larger than  $7 \text{ km}^2$ ,  
 738 which account for roughly 83% of the study area, are shown. **(b)** Relative contributions (%) of  
 739 the uncertainties in the projected changes at each of these watersheds; Hydro = Hydrologic models;  
 740 Para = hydrologic model parameters; GCM = General Circulation Models; RCP = Representative  
 741 concentration pathways (emission scenarios); “other” is the uncertainty from the 3<sup>rd</sup> and 4<sup>th</sup>  
 742 orders of interactions between the 4 major sources (i.e., GCMs, RCPs, Hydrologic models and  
 743 parameters).  
 744



745 **Figure 8:** Probability of changes in  $Q_m$ ,  $Q_p$  and  $Q_{100}$  at the Mission Creek watershed (No. 20 in  
 746 Figure 7 map). The numbers in the plot are the probabilities of positive changes in  $Q_m$ ,  $Q_p$  and  $Q_{100}$   
 747 (areas of shaded regions) under each emission scenario (blue numbers are for RCP 4.5 and red  
 748 numbers are for RCP 8.5).



749 **Figure 9: (a)** Projected change (days) in the onset and duration of wet season in SBC; positive  
750 (negative) values indicate later (earlier) onset or longer (shorter) duration of the wet season; **(b)**  
751 relative contributions (%) of the uncertainties of the projected changes in seasonality. Hydro =  
752 Hydrologic models; Para = hydrologic model parameters; GCM = General Circulation Models;  
753 RCP = Representative concentration pathways (emission scenarios); “other” is the uncertainty  
754 from the 3<sup>rd</sup> and 4<sup>th</sup> orders of interactions between the 4 major sources (i.e., GCMs, RCPs,  
755 Hydrologic models and parameters).